Building and Environment 94 (2015) 43–53

Contents lists available at ScienceDirect

Building and Environment

journal homepage: www.elsevier.com/locate/buildenv

A numerical study of particle deposition in ribbed duct flow with different rib shapes

Hao Lu, Lin Lu*

Department of Building Services Engineering, The Hong Kong Polytechnic University, Hung Hom, Kowloon, Hong Kong, China

ARTICLE INFO

Article history:
Received 26 May 2015
Received in revised form
9 July 2015
Accepted 23 July 2015
Available online 31 July 2015

Keywords:
Particle deposition
Surface ribs
Deposition enhancement
Rib shape
CFD

ABSTRACT

The effects of surface rib shapes on particle deposition in turbulent duct air flows were numerically studied based on the Reynolds stresses model (RSM) with UDF code correction and the discrete particle model (DPM). The shapes of the rib cross sections were square, triangular and circular. The ratios of rib height to duct diameter *e/D* were 0.1. The present air velocity distributions for both smooth and ribbed ducts as well as particle deposition velocity in a smooth duct are all in good agreement with previous related study data. An efficiency ratio has been defined to evaluate the particle deposition enhancement ratio together with the increase of flow drag. It is found that the square ribs have the maximum enhancement efficiency on particle deposition, compared with the other rib shapes. The maximum efficiency ratio can reach about 400 for small particles ($\tau_p^+ < 1$) but only about 2 for large particles ($\tau_p^+ > 1$) when the rib shape is square. Moreover, the mechanisms of particle deposition enhancement for different rib shapes were investigated and analyzed.

1. Introduction

Hazy weather is a serious problem in urban environment nowadays, especially in industrialized regions. The particulate matters (PM) in the air are much hazardous for people's health. Because they are commonly too small to exhaust from the lungs, such as PM2.5. Moreover, as people spend most of time indoors, the indoor air quality (IAQ) is particularly crucial for people's health. To improve the IAQ, it is necessary to develop high efficient particle removal devices. Suh and Kim found that the removal performance can be significantly enhanced by arrangement of repeated surface ribs on air electrostatic precipitators (ESP) due to particle deposition enhancement [1]. Lai et al. [2–5] also proposed that arrangement of repeated surface ribs on a length of the ventilation duct can obviously enhance airborne particle deposition for the IAQ filtration. If amount of aerosol particles can be collected and deposited in a length of dismountable ventilation duct, the IAQ would be significantly improved which is favorable for people's health. In a previous study conducted by the authors [6], it was found that particle deposition could be significantly enhanced for several orders of magnitude by rib interception and the entrainment of turbulent eddies. Nevertheless, the negative effect of the surface ribs is the increase of the air flow drag. Therefore, it is important and valuable to design the rib parameters for high particle deposition enhancement with low flow drag increase.

Over the past few decades, several studies have been carried out on particle deposition enhancement by surface ribs. Lai et al. [2–5] experimentally investigated particle deposition enhancement in turbulent duct air flows by two- and three-dimensional surface ribs. The cross section shape of the ribs is square. They found that particle deposition rate would be significantly enhanced by the surface ribs. Barth et al. [7] investigated particle-laden air flow in ribbed duct with square rib cross section by experiment. However, the particle deposition enhancement was not investigated. Recently, numerical simulation based on computational fluid dynamics (CFD) has been becoming one of the main methods to investigate particle deposition in turbulent air flow [8]. Because numerical simulation can predict the airflow fields, particle deposition and behavior in details [9–11]. Li et al. [12] investigated the particle deposition in obstructed duct flows. It was found that a large number of particle are intercepted by the blocks. Iacono et al. [13] predicted spherical and non-spherical particle deposition in ribbed duct flows by large eddy simulation (LES). The cross section shape of the ribs is also square. The results showed that spherical particles are preferentially concentrated on the windward rib surface while non-spherical particles don't. Lecrivain et al. [14]

* Corresponding author.
E-mail address: vivien.lu@polyu.edu.hk (L. Lu).

http://dx.doi.org/10.1016/j.buildenv.2015.07.030
0360-1323/

predicted multilayer particle deposition in square ribbed channel flow by Reynolds-averaged Navier–Stokes (RANS) model. The results showed good agreement with experimental test data. Therefore, the previous studies indicate that the CFD method can successfully predict particle deposition process in complicated turbulent air flow. It has been found that the surface ribs can enhance the particle deposition rate significantly [2–7]. Nevertheless, the shape of surface rib is commonly square in the previous studies. The influences of different rib shapes on particle deposition as well as the flow drag increase have been not investigated. But it can be concluded that the rib shapes may have important influences on the turbulent flow fields and the particle deposition behaviors. Therefore, this study aims to numerically study the particle deposition performance in ribbed duct air flows with different rib shapes.

Reasonable numerical models are crucial for simulating correctly the particle deposition process. Generally, there are three numerical methods for turbulent flow simulation: Direct numerical simulation (DNS), Large Eddy Simulation (LES) and Reynolds-averaged Navier–Stokes simulation (RANS). For DNS or LES, the computational cost is too high for engineering application although they have higher accuracy. Moreover, it had been widely proved that RANS model with velocity fluctuation correction can already accurately predict particle deposition process with 0.1–50 μm in turbulent flow [15–19]. Therefore, Reynolds stress model (RSM) with velocity fluctuation correction, which considers turbulence anisotropy, is adopted in this simulation because it can obtain more accurate particle deposition velocity than other RANS models [20,21]. For particle phase simulation, discrete particle model (DPM) is employed to track the movement trajectory of each particle. The objective of this study is to investigate and evaluate the effects of rib shapes on particle deposition enhancement performance with different particle sizes. Moreover, the mechanisms of particle deposition enhancement by ribbed surface are also studied and discussed.

2. Numerical model and methodology

In this study, the particle deposition process in ribbed duct turbulent flow was simulated based on the commercial software Ansys Fluent 13.0 with user-defined function (UDF) code correction.

2.1. Turbulent air flow model

As discussed in Introduction, the RSM model with velocity fluctuation correction were adopted to simulate turbulent duct flow fields. The governing equations of the mass conservation, the momentum conservation, the Reynolds stress transport and the turbulence dissipation rate transport for incompressible turbulence can be found in the literature [6,22], which are not clarified again here.

Near-wall modeling for air duct flow is important for accurately predicting deposition velocity of particles [20]. In this study, the two-layer zonal model combined with enhanced wall function was adopted to deal with the near-wall turbulent flow [23]. The turbulent viscosity and the dissipation rate ε is computed by,

$$\mu_{t,2layer} = \rho C_\mu l_\mu \sqrt{k} \tag{1}$$

$$\varepsilon = \frac{k^{3/2}}{l_\varepsilon} \tag{2}$$

More details of the model can be found in Ansys Fluent 13 [24].

To impose a fully developed velocity and T.K.E. profiles, user-defined boundary conditions were used in duct inlet. The Prandtl's one seventh power law was employed to describe the fully developed duct air velocity profiles [20],

$$U = U_{free}\left(\frac{y}{D/2}\right)^{1/7} \quad \text{for } y \le D/2 \tag{3}$$

$$U = U_{free}\left(\frac{h-y}{D/2}\right)^{1/7} \quad \text{for } y > D/2 \tag{4}$$

$$U_{free} = \frac{8}{7}U_{mean} \tag{5}$$

where U_{mean} is the mean velocity of the duct air flow and D is the duct height. The turbulent kinetic energy (T.K.E.) at the inlet was assumed to vary linearly from the near-wall value. The T.K.E. profiles [20] are given by,

$$k = \frac{\tau_w}{\rho_g\sqrt{C_\mu}} + \frac{y}{D/2}\left(0.002U_{free}^2 - \frac{\tau_w}{\rho_g\sqrt{C_\mu}}\right) \quad \text{for } 0 \le y \le D/2 \tag{6}$$

$$k = \frac{\tau_w}{\rho_g\sqrt{C_\mu}} + \frac{D-y}{D/2}\left(0.002U_{free}^2 - \frac{\tau_w}{\rho_g\sqrt{C_\mu}}\right) \quad \text{for } D/2 < y \le D \tag{7}$$

$$\tau_w = \frac{\rho_g U_{mean}^2}{2}\cdot f \tag{8}$$

where f is the fanning friction factor and is computed by,

$$f = 0.0791\cdot \mathrm{Re}^{-0.25}\left(2,800 < \mathrm{Re} < 105^2\right) \tag{9}$$

where Reynolds number Re is defined as,

$$\mathrm{Re} = \frac{U_{free}h}{\nu} \tag{10}$$

2.2. Particle motion model

Discrete particle model (DPM) was employed to simulate particle motion in the study. The modification of particles on turbulent air flow and the interactions between particles are ignored. Because the particle concentration in this study is very dilute. In the air-particle flow, the particle forces include drag force, gravity force, buoyancy force, pressure gradient force, Basset force, virtual mass force, Brownian force, and Saffman's lift force [25]. However, the ratio of air density to particle density is so small (in this study, it is 0.0005) that the pressure gradient force, the Basset force and the virtual mass force can be neglected, compared with the external force on particles [25]. Therefore, the drag force, the gravity force, the buoyancy force, the Brownian force and the Saffman's lift force are considered in this simulation. The particle-phase governing equation can be written by,

$$\frac{du_p}{dt} = \frac{1}{\tau}\frac{C_D\mathrm{Re}_p}{24}\left(u_g - u_p\right) + \frac{g\left(\rho_p - \rho_g\right)}{\rho_p} + F_B + F_S \tag{11}$$

where u_g and u_p are the velocity of fluid and particle, respectively. ρ_g

is the density of fluid and ρ_p is the density of particle. The drag force, the gravity force, the buoyancy force, the Brownian force F_B and the Saffman's lift force F_S are considered in the model. The Brownian force F_B is calculated by,

$$F_B = \zeta\sqrt{\frac{\pi S_0}{\Delta t}} \tag{12}$$

where $S_0 = \frac{216\rho\nu k_b T}{\pi\rho_p^2 d_p^5 C_C}$. The Saffman's lift force F_S is written as follows,

$$F_S = \frac{2\rho K_c \nu^{0.5}}{\rho_p d_p (S_{lk}S_{kl})} s_{ij}(u - u_p) \tag{13}$$

The particle relaxation time is given by,

$$\tau = \frac{Sd_p^2 C_C}{18\nu} \tag{14}$$

S is the ratio of particle-to-fluid density. The Cunningham slip correction factor C_C is calculated by Ref. [26],

$$C_C = 1 + \frac{2\lambda}{d_p}\left(1.257 + 0.4e^{-(1.1d_p/2\lambda)}\right) \tag{15}$$

The drag coefficient C_D is given as,

$$C_D = \frac{24}{\mathrm{Re}_p}, \quad \text{for } \mathrm{Re}_p < 1 \tag{16}$$

and

$$C_D = \frac{24}{\mathrm{Re}_p}\left(1 + 0.15\mathrm{Re}_p^{0.687}\right), \quad \text{for } 1 < \mathrm{Re}_p < 400 \tag{17}$$

2.3. Turbulent dispersion of particles

Turbulent particle dispersion has significantly influence on particle deposition and transport [20]. In the present study, Discrete Random Walk model (DRW) [24], which allows successive encounter of particles with turbulent eddies by a Gaussian distributed random velocity fluctuation of fluids and a time scale of turbulent eddy, was employed to deal with turbulent dispersion of particles.

The instantaneous turbulent fluctuating velocity is obtained by,

$$u' = \zeta u'_{rms}, \quad v' = \zeta v'_{rms}, \quad w' = \zeta w'_{rms} \tag{18}$$

where ζ is normal distributed random number; and u'_{rms}, v'_{rms} and w'_{rms} in Eq. (23) are velocity fluctuation.

It was found that the turbulent velocity fluctuation in the wall-normal direction is important for predicting particle deposition process [20,21]. To accurately simulate particle deposition in smooth duct, velocity fluctuation was corrected according to the DNS data by Kim et al. [20,27]:

$$\frac{v'_{rms}}{u^*} = C\left(y^+\right)^2, \quad \text{for } y^+ < 4 \tag{19}$$

where u^* is the friction velocity, and C is 0.008. y^+, defined as Eq. (25), is non-dimensional distance from the wall.

$$y^+ = \frac{yu^*}{\nu} \tag{20}$$

For particle deposition in ribbed duct, the correction Eq. (21) had been successfully applied in multilayer deposition simulation on ribbed channel flow by Lecrivain et al. [14]. This correction was also employed in the present simulation.

$$\frac{v'_{rms}}{u^*} = \frac{a_1 y^{+2}}{1 + b_1 y^+ + c_1 y^{+2.41}}, \quad \text{for } y^+ < 30 \tag{21}$$

where $a_1 = 0.0116$, $b_1 = 0.203$ and $c_1 = 0.0014$.

2.4. Particle deposition velocity

The particle deposition process is commonly evaluated by particle deposition velocity, which is defined as:

$$V_d = \frac{J}{C_0} \tag{22}$$

where J is the number of particles deposited per unit time and unit area of the surface, and C_0 is the mean particle concentration. In the computation, the particle deposition velocity V_d can be calculated by,

$$V_d = \frac{N_d/t_d/A}{N_0/V} = \frac{N_d/t_{\max}}{N_0/h} \tag{23}$$

Particle deposition rate is commonly evaluated through the dimensionless particle deposition velocity versus dimensionless particle relaxation time [16]. The dimensionless particle deposition velocity can be given by,

$$V_d^+ = \frac{V_d}{u^*} \tag{24}$$

where frictional velocity u^* can be calculated by,

$$u^* = \sqrt{\tau_w/\rho_g} = U_{mean}\sqrt{f/2} \tag{25}$$

The dimensionless particle relaxation time can be calculated by,

$$\tau_p^+ = \frac{C_C S d_p^2 u^{*2}}{18\nu^2} \tag{26}$$

3. Case description

The two-dimensional (2D) computational ducts for both smooth and ribbed wall cases are shown in Fig. 1. For particle deposition on smooth wall, the airflow duct was designed as 0.02 m high and 0.4 m long as shown in Fig. 1(a). The duct size and the flow conditions were consistent with the literatures for validation. For particle deposition on ribbed walls, three different rib shapes were investigated and compared. The cross sections of the ribs were square, triangular and circular as shown in Fig. 1(b), (c) and (d) respectively. The duct sizes of ribbed ducts were the same with the smooth duct for comparison. To ensure the fully developed condition of the turbulent air flow, the first half of the duct was designed as smooth, while nine ribs were arranged on the second half of the duct walls with identical spacing in streamwise direction.

According to the literatures of heat transfer enhancement by surface ribs [28,29], the maximum enhancement of heat transfer with lowest pressure increase occurs when the rib spacing to rib height ratio p/e is around 10. Moreover, the rib height to duct diameter ratio is usually from 0.02 to 0.1 in heat transfer enhancement by surface ribs [28,29]. In this study, the ratio of the rib spacing to height p/e was also chosen as 10. The rib height to

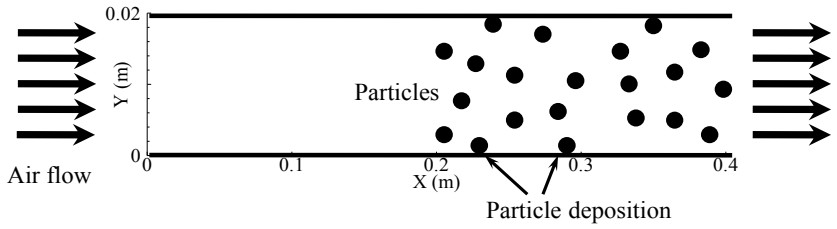

(a) Smooth-wall duct

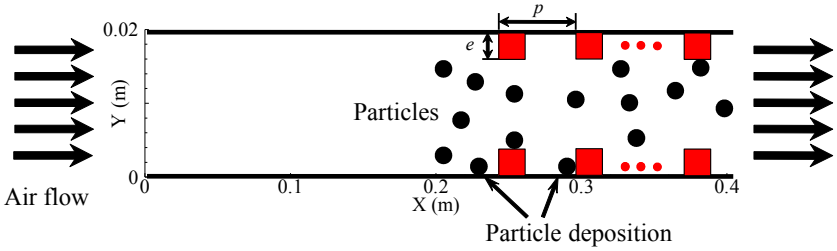

(b) Square ribbed-wall duct

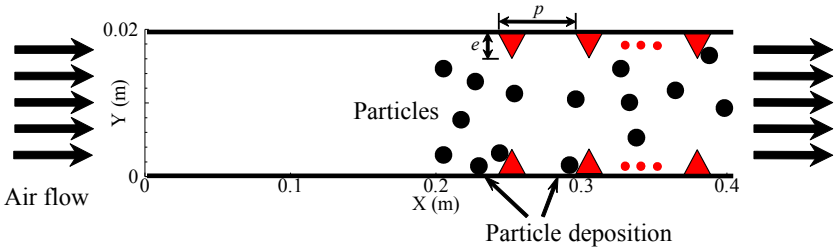

(c) Triangular ribbed-wall duct

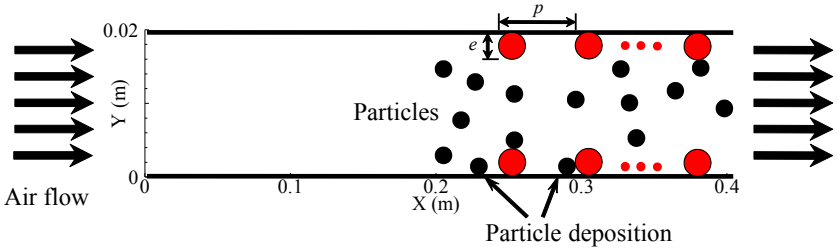

(d) Circular ribbed-wall duct

Fig. 1. Schematic view of particle deposition in smooth- and ribbed-wall ducts.

duct diameter ratio is 0.1. This is also in accordance with the experimental condition by Casara [30] for validating the flow fields in ribbed duct.

A total number of 32 cases were simulated in the study, as shown in Table 1. Eight particle sizes were studied in the simulation. They are 1, 2, 3, 5, 10, 20, 30 and 50 μm. In this study, The air dynamic viscosityμ is 1.789 $\times$ 10^{-5} kg s/m and the air density is 1.225 kg/m^3 at T = 288 K. The air velocity is 5.5 m/s. Thus the Reynolds number based on the mean flow velocity and duct height is 7534.

Structured grids were developed to discretize the calculated domain by the software Ansys ICEM 13.0 for both smooth and ribbed duct cases. The regional structured grids in the simulation for smooth and ribbed ducts are shown in Fig. 2. The grid numbers

Table 1
Computational cases.

Case no.	Air velocity (m/s)	Particle diameter (μm)	Surface type	Rib shape
A (1–8)	5.5 m/s	1,2,3,5,10,20,30,50	Smooth	–
B (9–16)	5.5 m/s	1,2,3,5,10,20,30,50	Ribbed	Square
C (17–24)	5.5 m/s	1,2,3,5,10,20,30,50	Ribbed	Triangle
D (25–32)	5.5 m/s	1,2,3,5,10,20,30,50	Ribbed	Circle

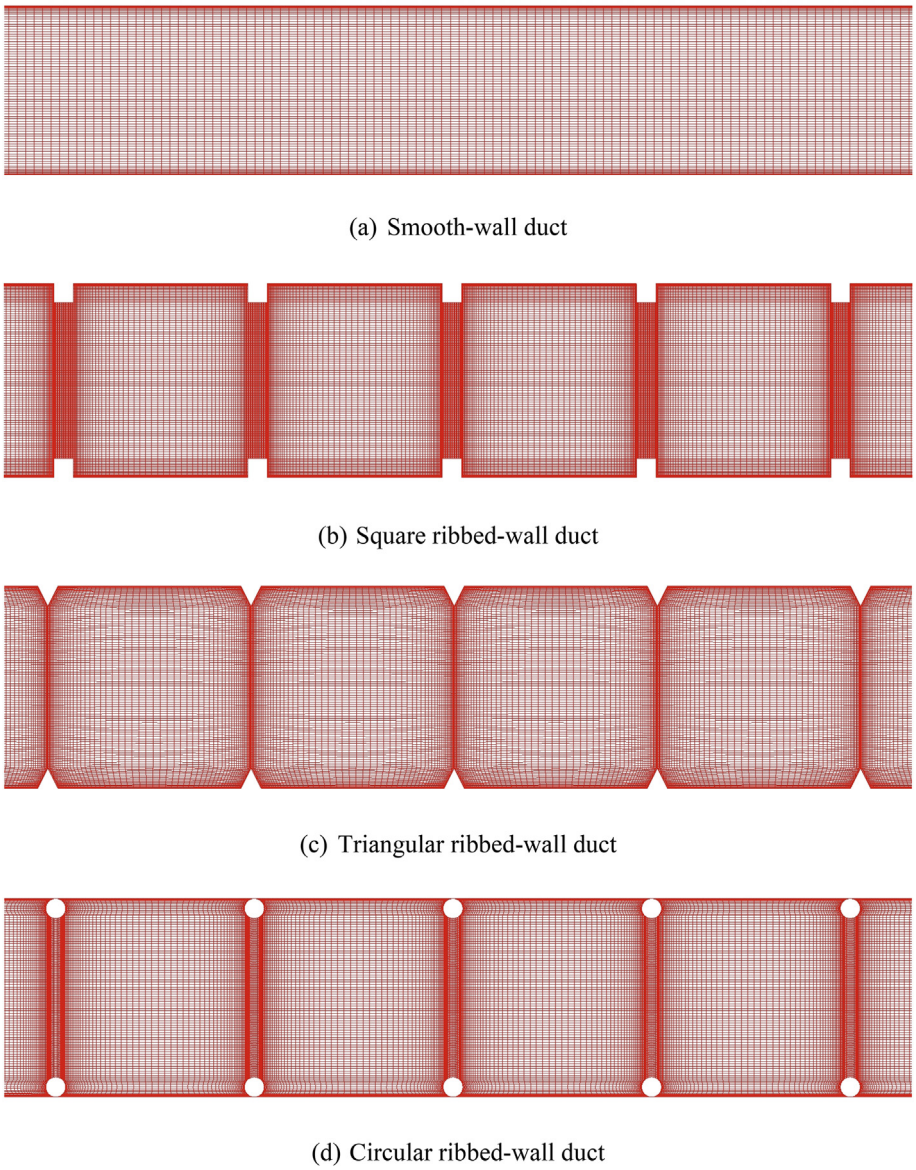

Fig. 2. Structural grid for smooth- and ribbed-wall ducts.

for Case A to Case D are 32,000, 101,251, 81,616 and 93,757, respectively. To accurately solve the complex turbulent flow in boundary layer, the grids were clustered near the ribs and walls. Tian and Ahmadi [20] detailed investigated the effects of different near-wall gird density on particle deposition simulation. They compared the computational results with the first gird point located at 0.1, 0.05, 0.01, 0.005, 0.001 and 0.0005 mm away from the wall. The study indicated that grid consistency was reached for the first gird spacing being at 0.05 mm. The corresponding dimensionless distance y^+ is about 1.13 wall units. The grid growing factor was selected as 1.2 from the wall to the core region in the wall-normal direction. The same grid resolution and sizes were employed in the present simulation.

The ratio of particle density to fluid density S is 2000. This is in accordance with the literatures [20,21]. Zhao et al. [31] investigated the influences of different particle numbers on particle deposition simulation results. The results showed that 1000 particles are large enough to achieve the statistically stable results. In this study, 30,000 spherical particles were released into the flow fields after the turbulent duct air flow had been calculated to be convergent. The particle release position was at $X = 0.2$ because the air flow had been in fully developed state there. The initial particle velocities were equal to the air mean velocity and the gravity force is parallel with the streamwise direction. In the simulation, the inlet and outlet boundary conditions for the particles are “Escape”, and the boundary conditions on the walls and the ribs for the particles are “Trap” [31]. In this study, the particle rebound and re-suspension are not considered. It is assumed that all the particles will be attached to the surface and never be re-suspended once they impact the walls and ribs.

The finite volume method (FVM) was employed to solve the fluid governing equations. The convection term was discretized by second-order upwind scheme and the diffusion terms were discretized by second-order central difference scheme. The Semi-Implicit Method for Pressure Linked Equations (SIMPLE) algorithm [32] was adopted to decouple the pressure and velocity fields. The Runge–Kutta method was adopted to solve the particle motion equations. The corrections of the turbulent velocity

fluctuations for smooth and ribbed wall cases as well as the inlet velocity and T.K.E distributions were imposed into FLUENT by UDF codes.

4. Results and discussion

4.1. Air-particle flow simulation and validation

The air flow fields in smooth and ribbed ducts were simulated and shown in Fig. 3. From the figure, it can be clearly observed the turbulent boundary layers over smooth and ribbed walls. The flow structures near the walls are significantly modified due to the disturbance of the surface ribs. The boundary layer is shifted by a distance away from the walls because of the surface ribs. Moreover, the recirculation zones in the cavities between adjacent surface ribs are also correctly simulated, as shown in Fig. 3(b) to (d).

Moreover, the air flow velocity profiles of both smooth and ribbed duct cases were validated quantificationally. For smooth duct case, Fig. 4 shows the comparison of the present mean and fluctuating air velocities with DNS data by Kim et al. [27]. The mean and fluctuating air velocities were obtained at X = 0.3 m as the flow had been in full development condition at that position. It can be observed that the present mean air velocity is in very good agreement with the DNS data, from Fig. 4(a). Moreover, the calculated fluctuating velocity profiles for streamwise and wall-normal directions agree also well with the literature results, as shown in Fig. 4(b). The above agreements indicate that the turbulent air flow fields for smooth duct case are resolved very well and correctly.

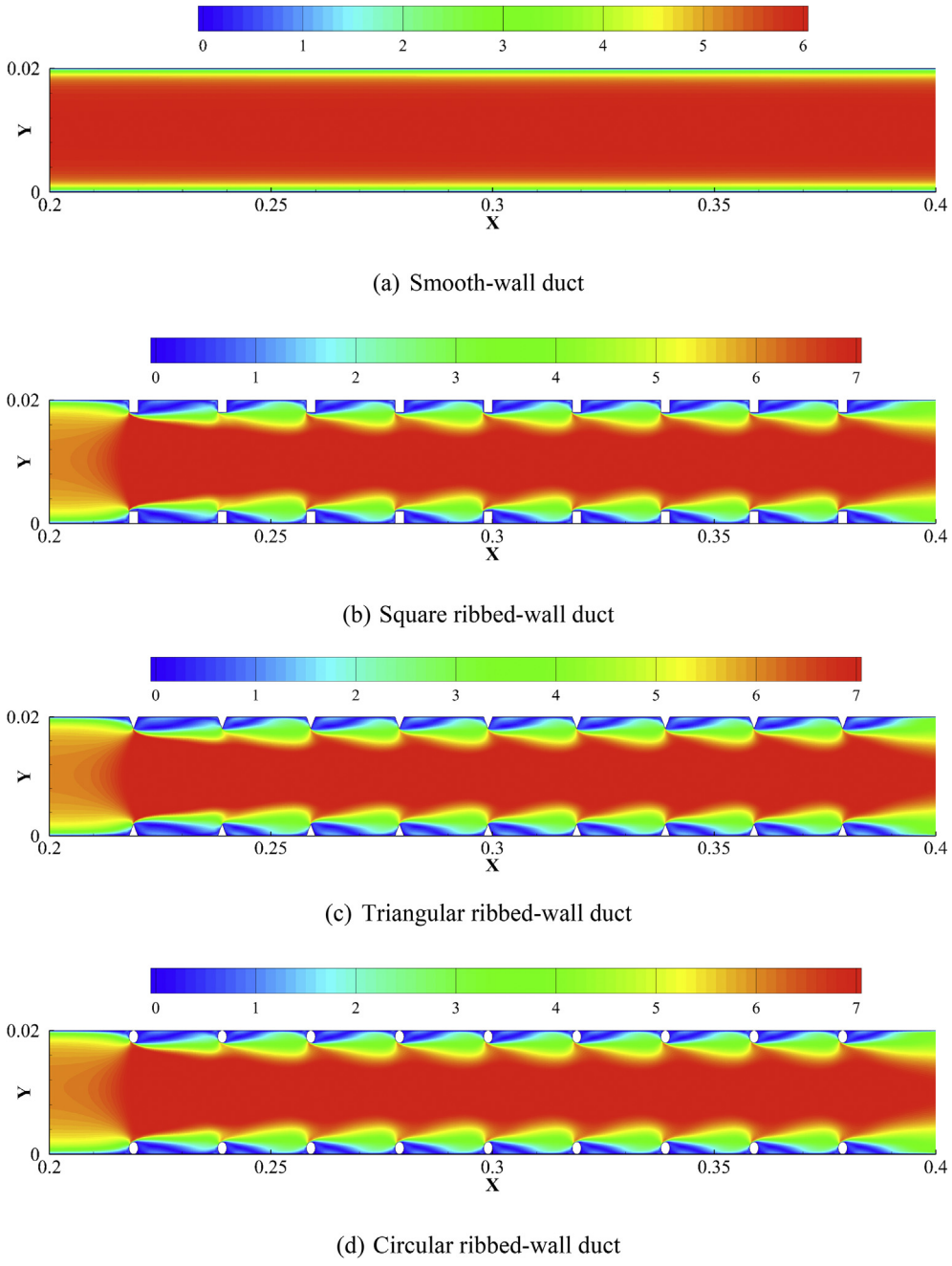

Fig. 3. Velocity fields of smooth- and ribbed-wall duct flows.

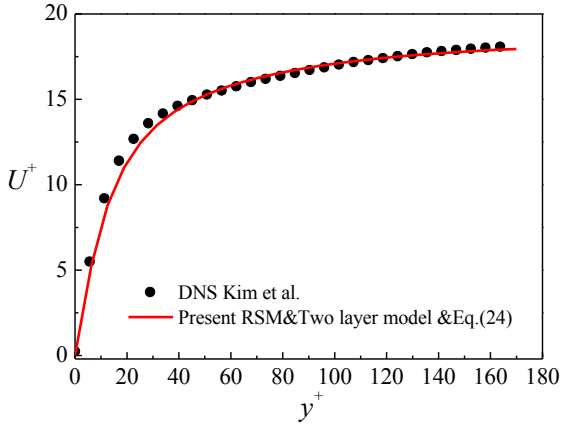

(a) Mean air flow velocity

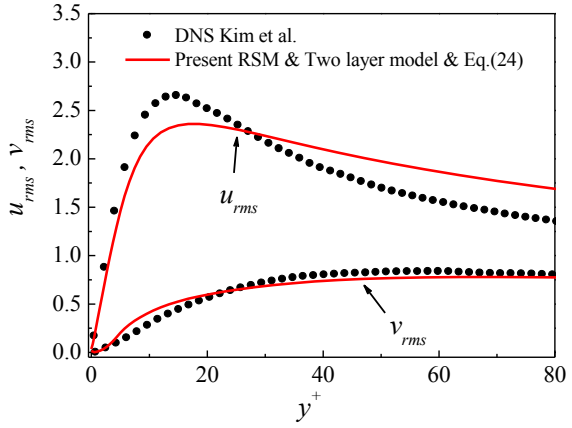

(b) Turbulent fluctuating velocity

Fig. 4. Validation of velocity profiles for smooth duct flow with DNS data.

Besides, the air velocity distributions for square ribbed duct case were also validated with experimental measurement data from the literature [30], as shown in Fig. 5. The air velocities were obtained from ten streamwise positions between the 8th and 9th ribs. From the Fig. 5, it can be seen that the velocity distributions obtained from present simulation are in good agreement with the experimental data. This implies that turbulent flow over square ribbed wall can be simulated well by the RSM with turbulent fluctuating velocity correction. Therefore, from the above verifications, it can be concluded that the turbulent air flow fields for both smooth and ribbed duct cases are all accurately resolved by the present CFD models.

Further, the particle deposition process in smooth duct was also verified. Fig. 6 shows the comparison of particle deposition velocity

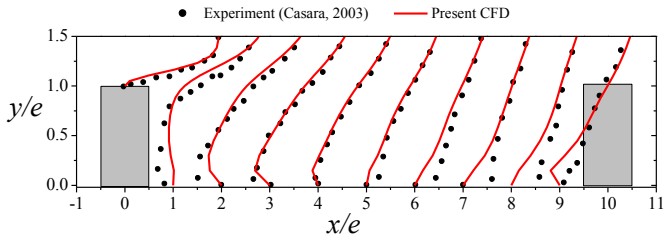

Fig. 5. Validation of velocity profiles for square ribbed duct flow with experimental data.

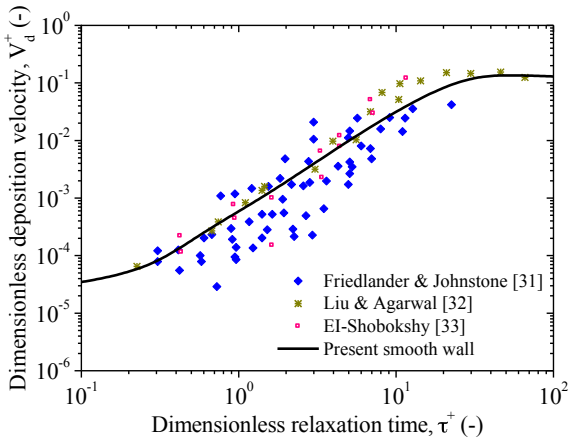

Fig. 6. Validation of particle deposition velocity in smooth-wall duct flow.

with the literature results [33–35] for smooth duct case. The non-dimensional deposition velocity was normalized by frictional velocity of air flow and the non-dimensional particle relaxation time was calculated by Eq. (19). From Fig. 6, it can be seen that the non-dimensional particle deposition velocity first increases dramatically with the increase of non-dimensionless particle relaxation time, and then almost keeps constant. This is because the particle inertia is enhanced with the increase of particle relaxation time, and the role of turbulent eddy capture and entrainment becomes weak for large particles. Moreover, the present calculated particle deposition velocity is highly consistent with the experimental data. Therefore, the present numerical methods can accurately predict particle deposition process.

4.2. Effects of rib shapes on particle deposition

To study the influences of rib shapes on the deposition velocity of particles, Fig. 7 shows the particle deposition velocities in smooth duct case and ribbed duct cases with different rib shapes. From the figure, it can be seen that the particle deposition velocity is obviously enhanced by the surface ribs. However, the enhancement ratios are quite different for different particle relaxation time. When the particle relaxation time is small ($\tau_p^+ < 1$), the enhancement ratio of particle deposition velocity can reach three or four orders of magnitude. Nevertheless, it can be only one or two orders of magnitude when the particle relaxation time is large ($\tau_p^+ > 1$).

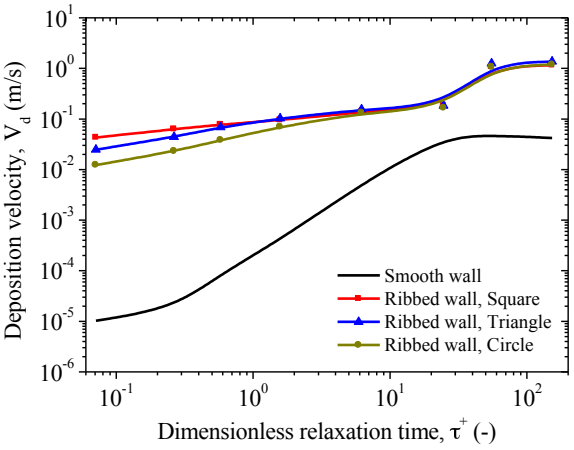

Fig. 7. Particle deposition velocities for ribbed-wall ducts with different rib shapes.

Compared with large particles ($\tau_p^+ > 1$), the deposition enhancement for small particles ($\tau_p^+ < 1$) is much effective. The reason is that the small particles are much more easily captured and entrained to the walls and ribs by the turbulent eddies. However, this mechanism is not efficient for large particles due to its large inertia. The detailed mechanism of particle deposition enhancement for different rib shapes is discussed in the Section 5.

To clearly observe the enhancement of particle deposition rate for different rib shapes, an enhancement ratioγ was defined as Eq. (27) and the results are shown in Fig. 8.

$$\gamma = \frac{v_{d\ rough}}{v_{d\ smooth}} \tag{27}$$

Theγ is the ratio of the dimensional particle deposition velocities between smooth and ribbed duct cases. It represents the pure enhancement of particle deposition by surface ribs without considering the flow drag increase. The comprehensive efficiency of particle deposition by the ribbed walls was investigated and discussed in the section below.

From Fig. 8, it can be found that the enhancement ratios of particle deposition velocity are influenced by the rib shapes only for$\tau_p^+ < 1$, but almost the same for$\tau_p^+ > 1$. The maximum enhancement ratio is obtained for square ribs (Case B). The maximum particle deposition enhancement ratio can reach about 4200 times for particle diameter 1 μm. Nevertheless, the minimum enhancement ratio of particle deposition is only about 4 times for particle diameter 20 μm. Therefore, it indicates that the particle deposition enhancement is much more efficient for small particles, especially for PM2.5.

4.3. Particle deposition efficiency ratio

As discussed above, the surface ribs can enhance particle deposition rate significantly. However, the air flow drag is also increased by the ribs, which means more power should be supplied for the flow system. In the practical engineering application, it is necessary to simultaneously evaluate the both effects. Therefore, a particle deposition efficiency ratioη for ribbed wall is defined by Eq. (28),

$$\eta = \frac{v_{d\ rough}}{v_{d\ smooth}} \cdot \frac{f_{smooth}}{f_{rough}} \tag{28}$$

where the parameter f_{rough}/f_{smooth} represents the increase of flow drag.

For smooth duct case, the flow drag of the second half duct is 0.0732 N, while they are 0.7207, 0.8394 and 0.6356 N for square, triangular and circular ribs, respectively. Therefore, the increase ratios of flow drag for the three ribbed ducts are respectively 9.8, 11.5 and 8.7, compared with the smooth duct case. The triangular ribs have the maximum flow drag while the circular ones have the minimum flow drag. Fig. 9 shows the efficiency ratio of particle deposition enhancement for different rib shapes. It can be found that the efficiencies of the ribbed duct cases are almost overlapped for$\tau_p^+ > 1$. When$\tau_p^+ < 1$, there are differences on the efficiencies between the three rib shapes. The efficiency ratio for square ribs is higher than those for the other two rib shapes. This is because the particle deposition enhancement ratio is the highest while the increase of flow drag is not so large for square ribs. In this study, the maximum efficiency ratio of particle deposition enhancement can reach about 400 for small particles ($\tau_p^+ < 1$). Therefore, square ribs are an efficient and effective alternative for particle deposition enhancement, especially for small particles ($\tau_p^+ < 1$).

5. Mechanisms of deposition enhancement for different rib shapes

In this section, the mechanisms of particle deposition enhancement by surface ribs with different shapes are investigated and discussed.

Firstly, the interception by the rib windward surface is an important mechanism for particle deposition enhancement. This mechanism was also described by Li et al. [12] and Lai et al. [2–5]. The number of intercepted particles is directly related to the rib height. As the heights of the three ribs are the same, the particle deposition enhancement by this mechanism is very similar for different rib shapes.

Secondly, the deposition area is increased due to the arrangement of the surface ribs. This is also favorable for particle deposition enhancement. Nevertheless, the increase ratios of deposition area are discrepant for different rib shapes. For smooth duct case, the two-dimensional total deposition area is 0.4 m. For ribbed duct cases, the two-dimensional increase of deposition area is 0.072, 0.044 and 0.077 m for square, triangular and circular ribs, respectively. Therefore, the increase ratios of deposition area are 18%, 11%, and 19.25% for ribbed duct Cases B to D, respectively. This indicates that the square and circular ribs have very similar deposition area increase. However, the increase of deposition area for triangular ribs is significantly low compared with the other two rib shapes.

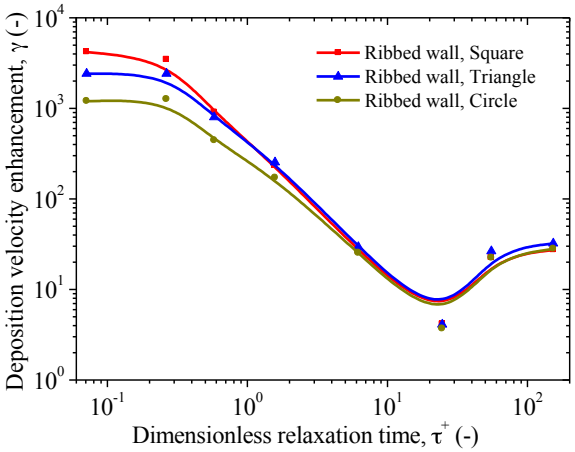

Fig. 8. Particle deposition enhancement by surface ribs with different shapes.

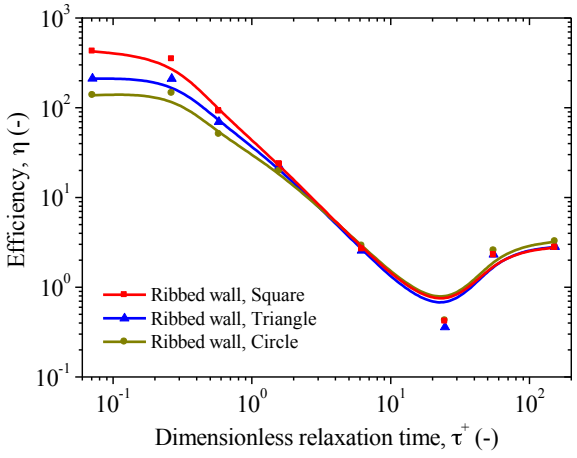

Fig. 9. Efficiency ratio of particle deposition enhancement by surface ribs with different shapes.

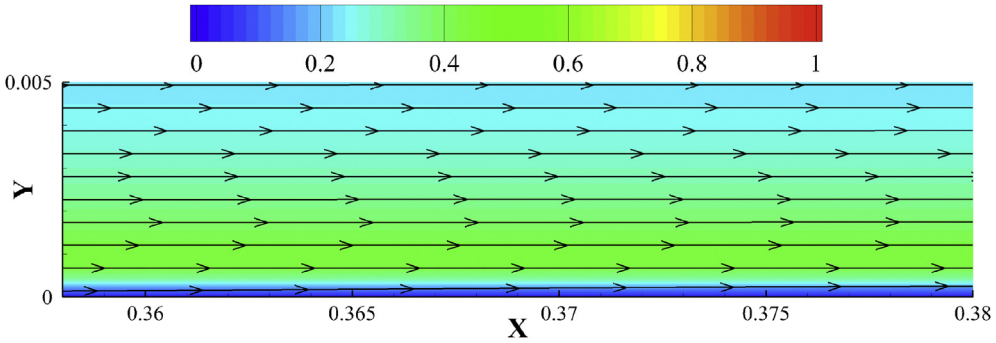

(a) Smooth-wall duct

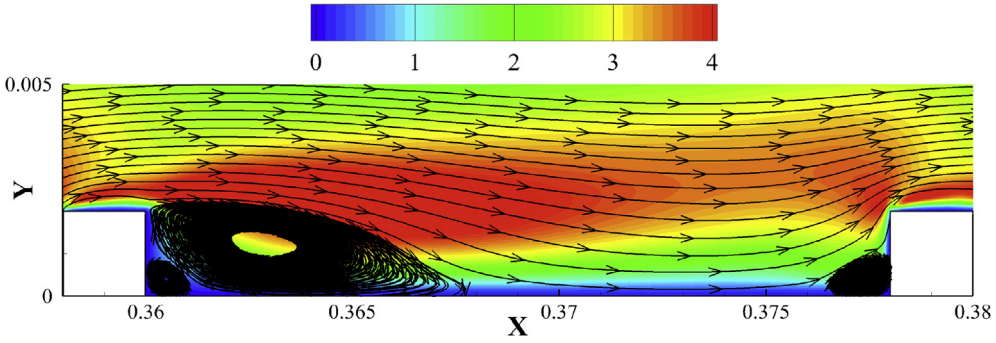

(b) Square ribbed-wall duct

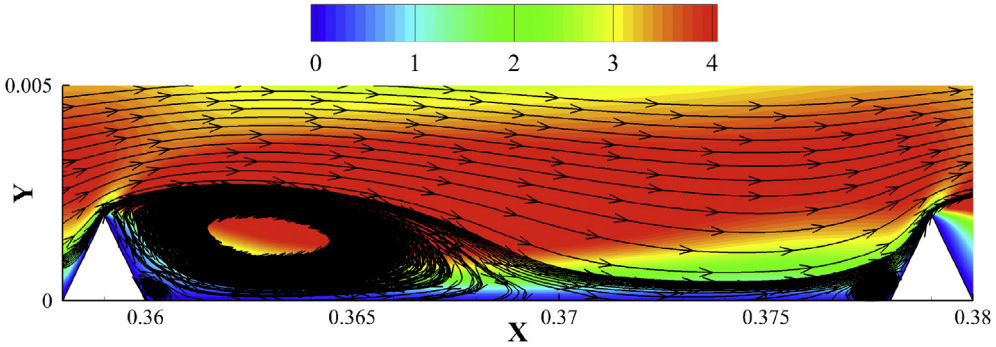

(c) Triangular ribbed-wall duct

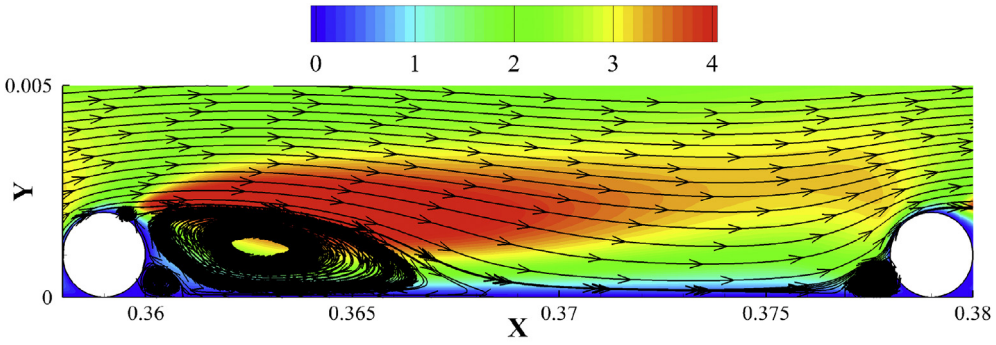

(d) Circular ribbed-wall duct

Fig. 10. T.K.E distribution and streamlines of air flow in smooth- and ribbed-wall ducts.

Finally, turbulent eddies and large turbulent kinetic energy (T.K.E) are induced by the introduction of surface ribs. A large number of particles will be captured by the turbulent eddies and entrained to the walls and ribs. To describe this mechanism clearly, turbulent kinetic energy (T.K.E) distribution overlaid the flow streamlines are shown in Fig. 10 for smooth and ribbed duct cases. It can be observed that the turbulent structures for ribbed duct cases are quite different to those for the smooth duct case. In the latter case, the flow is completely along the streamwise direction and the near-wall T.K.E value is very small. These are not favorable conditions for particle deposition. For ribbed ducts, there are a large separation eddy and a small attachment eddy in the cavity, which cause intense momentum exchange between the outer flow and the cavity flow. It can be also noted that the T.K.E. in the cavity is much larger, compared with the smooth duct case. Obviously, the strong momentum exchange and large T.K.E. value near the wall are beneficial for particle deposition, as many particles would be captured by the turbulent eddies and entrained to the wall for deposition. From Fig. 10, it can found that the turbulent eddies and T.K.E values near the ribs are different for different rib shapes. The largest eddies and near-wall T.K.E distribution are induced by the triangular ribs, the second largest is for square ribs, and the smallest is for circular ribs. This conclusion is consistent with the literature results for heat transfer enhancement by different rib shapes [36].

Therefore, the triangular ribs have the smallest deposition area increase while the weakest turbulent eddies and T.K.E are induced by the circular ribs. Nevertheless, the square ribs have both good performance on the above two mechanisms. Thus the maximum particle deposition enhancement is obtained by the square ribs for small particles ($\tau_p^+ < 1$). However, the capture and entrainment effects by turbulent eddies are very weak for large particles ($\tau_p^+ > 1$) because of their larger inertias. The main deposition enhancement mechanism for large particles is the interception of surface ribs. Therefore, the particle deposition enhancement for different rib shapes is very similar for large particles ($\tau_p^+ > 1$).

6. Conclusions

In the study, the influences of surface rib shapes on particle deposition enhancement were numerically investigated for different particle sizes. The efficiencies and mechanisms of particle deposition enhancement were analyzed and discussed based on the RSM with UDF corrections and DPM model. The following conclusions can be obtained,

1. Particle deposition velocity is significantly enhanced by the introduction of the surface ribs. For small particles ($\tau_p^+ < 1$), the enhancement ratio of particle deposition velocity can reach three or four orders of magnitude due to the capture and entrainment of turbulent eddies. Nevertheless, it can be only one or two orders of magnitude for large particles ($\tau_p^+ > 1$) because of the large inertias.
2. Compared with triangular and circular ribs, the square ribs have the maximum enhancement on particle deposition for small particles ($\tau_p^+ < 1$). This is because the square ribs have the best comprehensive performances on the deposition area increase ratio, the turbulent eddies production and the near-wall T.K.E enhancement. However, as the main deposition enhancement mechanism for large particles ($\tau_p^+ > 1$) is the interception of surface ribs, there are almost no difference on the particle deposition velocity between the three kinds of surface ribs for large particles ($\tau_p^+ > 1$).
3. The maximum efficiency ratio of particle deposition is obtained for square surface ribs, compared with the other two rib shapes. The maximum efficiency ratio can reach about 400 for small particles ($\tau_p^+ < 1$) but only about 2 for large particles ($\tau_p^+ > 1$) when the rib shape is square.

Therefore, the arrangement of square ribs on the walls is an efficient and effective way to enhance the particle deposition, which can be applied in the air filtration devices.

In addition, the three-dimensional (3D) simulation of particle deposition in ribbed duct air flows and the according experimental validation should be conducted in future work. Moreover, the re-suspension of the deposited particles in the duct flow may change the particle deposition rate. This influence also needs to be further studied [37].

Acknowledgment

The authors appreciate the financial supports provided by Central Policy Unit of the Hong Kong Government via the Public Policy Research Scheme (2013.A6.010.13A).

References

[1] J.H. Vincent, A.S.M. MacLennan, Aerodynamic considerations in electrostatic precipitator, J. Electrost. 8 (1980) 325–342.
[2] A.C.K. Lai, M.A. Byrne, A.J.H. Goddard, Measured deposition of aerosol particles on a two-dimensional ribbed surface in a turbulent duct flow, J. Aerosol Sci. 30 (1999) 1201–1214.
[3] A.C.K. Lai, M.A. Byrne, A.J.H. Goddard, Enhanced particle loss in ventilation duct with ribbed surface, Build. Environ. 35 (2000) 425–432.
[4] A.C.K. Lai, M.A. Byrne, A.J.H. Goddard, Aerosol deposition in turbulent channel flow in a regular array of three dimensional roughness elements, J. Aerosol Sci. 32 (2001) 121–137.
[5] A.C.K. Lai, M.A. Byrne, A.J.H. Goddard, Particle deposition in ventilation duct onto three-dimensional roughness elements, Build. Environ. 37 (2002) 939–945.
[6] H. Lu, L. Lu, Numerical investigation on particle deposition enhancement in duct air flow by ribbed wall, Build. Environ. 85 (2015) 61–72.
[7] T. Barth, M. Reiche, M. Banowski, M. Oppermann, U. Hampel, Experimental investigation of multilayer particle deposition and resuspension between periodic steps in turbulent flows, J. Aerosol Sci. 64 (2013) 111–124.
[8] Q. Chen, Ventilation performance prediction for buildings: a method overview and recent applications, Build. Environ. 44 (4) (2009) 848–858.
[9] H. Jiang, L. Lu, K. Sun, Simulation of particle deposition in ventilation duct with a particle-wall impact model, Build. Environ. 45 (5) (2010) 1184–1191.
[10] K. Sun, L. Lu, H. Jiang, A computational investigation of particle distribution and deposition in a 90° bend incorporating a particle-wall model, Build. Environ. 46 (2011) 1251–1262.
[11] K. Sun, L. Lu, H. Jiang, A numerical study of bend-induced particle deposition in and behind duct bends, Build. Environ. 52 (2012) 77–87.
[12] A. Li, G. Ahmadi, R.G. Bayer, M.A. Gaynes, Aerosol particle deposition in an obstructed turbulent duct flow, J. Aerosol Sci. 25 (1994), 91–12.
[13] G.I. Iacono, P. Tucker, A. Reynolds, Predictions for particle deposition from LES of ribbed channel flow, Int. J. Heat. Fluid Flow. 26 (2005) 558–568.
[14] G. Lecrivain, S. Drapeau-Martin, T. Barth, U. Hampel, Numerical simulation of multilayer deposition in an obstructed channel flow, Adv. Powder Technol. 25 (2014) 310–320.
[15] N.P. Gao, J.L. Niu, Modeling particle dispersion and deposition in indoor environments, Atmos. Environ. 41 (2007) 3862–3876.
[16] N. Gao, J. Niu, Q. He, T. Zhu, J. Wu, Using RANS turbulence models and Lagrangian approach to predict particle deposition in turbulent channel flows, Build. Environ. 48 (2012) 206–214.
[17] H. Jiang, L. Lu, K. Sun, Computational fluid dynamics (CFD) modelling of particle deposition in a two-dimensional turbulent channel air flow: study of influence factors, Indoor Built Environ. 21 (2) (2012) 264–272.
[18] K. Sun, L. Lu, H. Jiang, Modelling of particle deposition and rebound behaviour on ventilation ducting wall using an improved wall model, Indoor Built Environ. 20 (3) (2011) 300–312.
[19] H. Jiang, L. Lu, K. Sun, Experimental study and numerical investigation of particle penetration and deposition in 90 degrees bent ventilation ducts, Build. Environ. 46 (2011) 2195–2202.
[20] L. Tian, G. Ahmadi, Particle deposition in turbulent duct flows-comparisons of different model predictions, J. Aerosol Sci. 38 (2007) 377–397.
[21] Z. Zhang, Q. Chen, Comparison of the Eulerian and Lagrangian methods for predicting particle transport in enclosed spaces, Atmos. Environ. 41 (2007) 5236–5248.
[22] B.E. Launder, G.J. Reece, W. Rodi, Progress in the development of a Reynolds stress turbulent closure, J. Fluid Mech. 68 (3) (1975) 537–566.
[23] H.C. Chen, V.C. Patel, Near-wall turbulence models for complex flows

including separation, AIAA J. 26 (1988) 641–648.
[24] FLUENT Inc, FLUENT 12.0 User's Guide, Lebanon, NH, 2009.
[25] B. Zhao, Y. Zhang, X.T. Li, X.D. Yang, D.T. Huang, Comparison of indoor aerosol particle concentration and deposition in different ventilated rooms by numerical method, Build. Environ. 39 (2004) 1–8.
[26] H. Ounis, G. Ahmadi, Analysis of dispersion of small spherical particles in a random velocity field, J. Fluids Eng. 112 (1990) 114–120.
[27] J. Kim, P. Moin, R. Moser, Turbulence statistics in fully developed channel flow at low Reynolds number, J. Fluid Mech. 177 (1987) 133–166.
[28] T.M. Liou, J.J. Hwang, S.H. Chen, Simulation and measurement of enhanced turbulent heat transfer in a channel with periodic ribs on one principal wall, Int. J. Heat. Mass Transf. 36 (1993) 507–517.
[29] T.M. Liou, W.B. Wang, Y.J. Chang, Holographic interferometry study of spatially periodic heat transfer in a channel with ribs detached from one wall, ASME Trans J Heat Transf. 117 (1995) 32–39.
[30] L. Casarsa, Aerodynamic Performance Investigation of a Fixed Rib-roughened Internal Cooling Passage, Ph.D. thesis, Von Karman Institute for Fluid Dynamics, Belgium, 2003.
[31] B. Zhao, C. Chen, X.Y. Yang, A.C.K. Lai, Comparison of three approaches to model particle penetration coefficient through a single straight crack in a building envelope, Aerosol Sci. Technol. 44 (2010) 405–416.
[32] S.V. Partankar, Numerical Heat Transfer and Fluid Flow, Hemisphere, Washington, DC, 1980.
[33] S.K. Friedlander, H.F. Johnstone, Deposition of suspended particles from turbulent gas streams, Ind. Eng. Chem. 49 (1957) 1151–1156.
[34] B.Y.H. Liu, J.K. Agarwal, Experimental observation of aerosol deposition in turbulent flow, J. Aerosol Sci. 5 (1974) 145–155.
[35] M.S. El-Shobokshy, Experimental measurements of aerosol deposition to smooth and rough surfaces, Atmos. Environ. 17 (1983) 639–644.
[36] M.A. Moon, M.J. Park, K.Y. Kim, Evaluation of heat transfer performances of various rib shapes, Int. J. Heat. Mass Transf. 71 (2014) 275–284.
[37] B. Zhou, B. Zhao, Z.C. Tan, How particle resuspension from inner surfaces of ventilation ducts affects indoor air quality-a modeling analysis, Aerosol Sci. Technol. 45 (2011) 996–1009.

Nomenclature

C_0: mean particle concentration
F_S: Saffman's lift force
D: duct height
f: fanning friction factor
f_{rough}: flow drag for rough duct
f_{smooth}: flow drag for smooth duct
J: number of particles deposited per unit time and unit area
k: turbulent kinetic energy (T.K.E.)
e: rib height
$\overline{p}$: time-averaged pressure
p: rib spacing
Re: Reynolds number
S: ratio of particle-to-fluid density
T_L: fluid Lagrangian integral time scale
U_{mean}: mean velocity of air
U_{free}: freestream velocity of air
u_g: velocity of fluid
$\overline{u}_i$: time-averaged velocity
u_p: velocity of particle
u'_{rms}: streamwise fluctuating velocity of air
V_d: particle deposition velocity
V_d^+: dimensionless particle deposition velocity
$v_{d\ rough}$: particle deposition velocity on ribbed duct
$v_{dsmooth}$: particle deposition velocity on smooth duct
v'_{rms}: wall-normal fluctuating velocity of air
w'_{rms}: spanwise fluctuating velocity of air
u^*: frictional velocity of air
y^+: dimensionless distance from the wall

Greek symbols

ε: dissipation rate of turbulent kinetic energy
ρ_g: density of fluid
ρ_p: density of particle
ζ: normal distributed random number
μ: dynamic viscosity of air
ν: kinetic viscosity of air
γ: ratio of dimensional particle deposition velocities between ribbed and smooth duct cases
η: a pressure drop-weighted particle deposition enhancement
τ_p^+: dimensionless particle relaxation time